Feb. 2007, revised version, submitted to JCP

CONTINUOUS GALERKIN METHODS FOR SOLVING THE TIME-DEPENDENT MAXWELL EQUATIONS IN 3D GEOMETRIES

Patrick Ciarlet, Jr

Laboratoire POEMS, UMR 2706 CNRS/ENSTA/INRIA,
École Nationale Supérieure de Techniques Avancées,
32, boulevard Victor, 75739 Paris Cedex 15, France
`patrick.ciarlet@ensta.fr`

Erell Jamelot

Laboratoire POEMS, UMR 2706 CNRS/ENSTA/INRIA,
École Nationale Supérieure de Techniques Avancées,
32, boulevard Victor, 75739 Paris Cedex 15, France
`erell.jamelot@ensta.fr`

A few years ago, Costabel and Dauge proposed a variational setting, which allows one to solve numerically the time-harmonic Maxwell equations in 3D geometries with the help of a continuous approximation of the electromagnetic field. In this paper, we investigate how their framework can be adapted to compute the solution to the time-dependent Maxwell equations. In addition, we propose some extensions, such as the introduction of a mixed variational setting and its discretization, to handle the constraint on the divergence of the field.

Introduction

We consider hereafter the discretization of the time-dependent electromagnetic field, governed by the Maxwell equations. More precisely, we are interested in building continuous approximations. Indeed, recall that it is advised, while solving the Maxwell-Vlasov system, to compute a continuous approximation of the field, especially when it is coupled to a Particle-In-Cell method[11,5]. Now, when one wants to compute a continuous, discrete field, it is well known that Maxwell's equations are accurately solved when the computational domain is either convex, or has a smooth boundary [5,6]. On the contrary, if the domain contains geometrical singularities, continuous finite elements span only a strict – closed – subset of all possible fields, which is made of the H^1-regular fields. In order to recover the total field in this situation, one can use several remedies, such as additional ansatz functions, introduce a weight, or relax the boundary condition. The first method, known as the singular complement method [4,22,21,3,14,24,25,2] works well in $2D$ and $2\frac{1}{2}D$ geometries. The second method, known as the weighted regularization method [19] works in $2D$ and $3D$. Finally, the third method has been studied only recently in 2D geometries [25].

Among the three methods, only one – the singular complement method – requires an explicit knowledge of the singular part of the fields (the part which is not H^1-regular). In this contribution[a], we examine some recent developments of the second method to solve the time-dependent Maxwell equations and we provide numerical results.

The outline of the paper is as follows. In the next Section, we recall the time-dependent Maxwell equations, which we express as a second-order in time system of equations. We also provide suitable initial and boundary conditions. In Section 2, we introduce some functional spaces. Then, we build a series of variational formulations in Section 3, which are equivalent to the original set of equations, under suitable assumptions. In Section 4, we propose a discretization of those variational formulations, based on a continuous approximation of the field. Then, in Section 5, we illustrate by two numerical examples the possibilities of this discretization techniques. Concluding remarks follow.

1. Setting of the problem

Let $\Omega \subset \mathbb{R}^3$ be a bounded, simply connected, open polyhedron with a Lipschitz, connected, boundary $\partial\Omega$. When the domain is non-convex, its boundary contains reentrant corners and/or edges, which are called geometrical singularities later on. Let $\mathbf{n}$ be the unit outward normal to $\partial\Omega$.

Let c, ε_0 and μ_0 be respectively the light velocity, the dielectric permittivity and the magnetic permeability ($\varepsilon_0\mu_0 c^2 = 1$). Over a time interval $]0, T[$, Maxwell's equations in vacuum read:

$$\partial_t \mathcal{E} - c^2 \, \mathbf{curl}\mathcal{B} = -\mathcal{J} \,/\, \varepsilon_0 \,, \tag{1.1}$$

$$\partial_t \mathcal{B} + \mathbf{curl}\mathcal{E} = 0 \,, \tag{1.2}$$

$$\mathrm{div}\mathcal{E} = \rho \,/\, \varepsilon_0 \,, \tag{1.3}$$

$$\mathrm{div}\mathcal{B} = 0 \,. \tag{1.4}$$

Above, $\mathcal{E}$ and $\mathcal{B}$ are the electric field and magnetic induction respectively, and ρ and $\mathcal{J}$ are the charge and current densities which satisfy the charge conservation equation:

$$\mathrm{div}\mathcal{J} + \partial_t \rho = 0 \,. \tag{1.5}$$

These quantities depend on the space variable $\mathbf{x}$ and on the time variable t.

In order to solve equations (1.1-1.4), one needs to define initial conditions (here at time $t = 0$):

$$\mathcal{E}(\cdot, 0) = \mathcal{E}_0 \,, \; \mathcal{B}(\cdot, 0) = \mathcal{B}_0, \tag{1.6}$$

[a]A short report appeared in the Proceedings of Enumath'05, see [15].

where the couple $(\mathcal{E}_0, \mathcal{B}_0)$ depends only on the variable $\mathbf{x}$. It is assumed that this initial data satisfies $\mathrm{div}\mathcal{E}_0 = \rho(0)\,/\,\varepsilon_0$ and $\mathrm{div}\mathcal{B}_0 = 0$.

The boundary is made up of two parts, $\partial\Omega = \overline{\Gamma}_C \cup \overline{\Gamma}_A$, where Γ_C is a perfectly conducting boundary, and Γ_A is an artificial boundary. Since the choice of the location of Γ_A is free, it is placed so that it does not cut nor contain any geometrical singularity [13]. Note that we do not require that $\partial\Gamma_A \cap \partial\Gamma_C = \emptyset$. We have:

$$\mathcal{E} \times \mathbf{n} = 0 \text{ and } \mathcal{B} \cdot \mathbf{n} = 0 \text{ on } \Gamma_C. \tag{1.7}$$

We further split the artificial boundary Γ_A into Γ_A^i and Γ_A^a. On Γ_A^i, we model incoming plane waves, whereas we impose an absorbing boundary condition on Γ_A^a. Both can be modelled [5] as a Silver-Müller boundary condition on Γ_A:

$$(c\mathcal{B} + \mathcal{E} \times \mathbf{n}) \times \mathbf{n} = c\,\mathbf{b} \times \mathbf{n} \text{ on } \Gamma_A, \text{ where } \mathbf{b} \text{ is given.} \tag{1.8}$$

The case of an absorbing boundary condition corresponds to $\mathbf{b} = 0$ in the above.

If we differentiate with respect to time (1.1) and add **curl** of (1.2) to it, we get a vector wavelike equation for $\mathcal{E}$, which reads

$$\partial_t^2 \mathcal{E} + c^2 \mathbf{curl}\,\mathbf{curl}\mathcal{E} = -\partial_t \mathcal{J}/\varepsilon_0.$$

Naturally, the initial value of $\partial_t \mathcal{E}$ is equal to $\mathcal{E}_1 := c^2\mathbf{curl}\mathcal{B}_0 - \mathcal{J}(.,0)\,/\,\varepsilon_0$. Recall that $\mathcal{E}$ is also *subject to* a constraint on its divergence, $\mathrm{div}\mathcal{E} = \rho\,/\,\varepsilon_0$. Next, it is easily seen, by using the trace of (1.2) on Γ_A, that

$$c^2\mathbf{curl}\mathcal{E} \times \mathbf{n} = c\,\partial_t(\mathcal{E} \times \mathbf{n}) \times \mathbf{n} - c^2\partial_t\mathbf{b} \times \mathbf{n} \text{ on } \Gamma_A.$$

We thus consider the following equivalent problem (PE):
Find $\mathcal{E}$ such that

$$\partial_t^2 \mathcal{E} + c^2 \mathbf{curl}\,\mathbf{curl}\mathcal{E} = -\partial_t\mathcal{J}/\varepsilon_0, \text{ in } \Omega,\, t \in]0,T[, \tag{1.9}$$

$$\mathrm{div}\mathcal{E} = \rho/\varepsilon_0, \text{ in } \Omega,\, t \in]0,T[, \tag{1.10}$$

$$\mathcal{E} \times \mathbf{n}_{|\Gamma_C} = 0,\, t \in]0,T[, \tag{1.11}$$

$$c^2\mathbf{curl}\mathcal{E} \times \mathbf{n}_{|\Gamma_A} = (c\,\partial_t(\mathcal{E} \times \mathbf{n}) \times \mathbf{n} - c^2\partial_t\mathbf{b} \times \mathbf{n})_{|\Gamma_A},\, t \in]0,T[, \tag{1.12}$$

$$\mathcal{E}(.,0) = \mathcal{E}_0, \text{ in } \Omega, \tag{1.13}$$

$$\partial_t\mathcal{E}(.,0) = \mathcal{E}_1, \text{ in } \Omega. \tag{1.14}$$

The same procedure can be carried out on the magnetic induction $\mathcal{B}$.

2. (Un)usual Sobolev spaces

In addition to the usual Lebesgue and Sobolev spaces, the building of the ad hoc variational formulations requires us to introduce some non-standard functional spaces when the domain is non-convex [19,13].

Let us begin with some Sobolev spaces, which are needed both in the convex and in the non-convex cases. Let $L^2(\Omega)$ (respectively $L^2(\partial\Omega)$) be the usual Lebesgue space of measurable and square integrable functions over Ω (resp. $\partial\Omega$). The usual norm and scalar product of $L^2(\Omega)$ are denoted by $||\cdot||_0$ and $(\cdot,\cdot)_0$, respectively. Then, $H^1(\Omega)$ will denote the space of $L^2(\Omega)$ functions with gradients in $L^2(\Omega)^3$. We then introduce two specialized spaces for the electromagnetic field:

$$\mathcal{H}(\mathbf{curl},\Omega) := \{\mathcal{F}\in L^2(\Omega)^3\,|\,\mathbf{curl}\mathcal{F}\in L^2(\Omega)^3\}\,,$$
$$\mathcal{H}_A(\mathbf{curl},\Omega) := \{\mathcal{F}\in\mathcal{H}(\mathbf{curl},\Omega)\,|\,\mathcal{F}\times\mathbf{n}_{|\partial\Omega}\in\mathcal{L}^2_t(\partial\Omega)\,,\,\mathcal{F}\times\mathbf{n}_{|\Gamma_C}=0\}\,.$$

Above, $\mathcal{L}^2_t(\partial\Omega):=\{\mathbf{u}\in L^2(\partial\Omega)^3\,|\,\mathbf{u}\cdot\mathbf{n}=0\text{ a. e.}\}$.

When Ω is convex, we introduce also

$$\mathcal{X}^A_\mathcal{E}:=\{\mathcal{F}\in\mathcal{H}_A(\mathbf{curl},\Omega)\,|\,\mathrm{div}\mathcal{F}\in L^2(\Omega)\}.$$

Under suitable data assumptions, it is known that $\mathcal{E}(t)\in\mathcal{X}^A_\mathcal{E}$. If $\Gamma_C=\partial\Omega$, we write simply $\mathcal{X}^0_\mathcal{E}$. According to Costabel [18], the graph norm and the semi-norm, $||\mathcal{F}||^2_{\mathcal{X}^0}=||\mathbf{curl}\mathcal{F}||^2_0+||\mathrm{div}\mathcal{F}||^2_0$ are equivalent norms on $\mathcal{X}^0_\mathcal{E}$. On $\mathcal{X}^A_\mathcal{E}$, one adds a third term, $||\mathcal{F}\times\mathbf{n}_{|\Gamma_A}||^2_{\mathcal{L}^2_t(\Gamma_A)}$, to recover an equivalent norm [20]. Also [1], $\mathcal{X}^0_\mathcal{E}$ is a subset of $H^1(\Omega)^3$: $\mathcal{X}^0_\mathcal{E}\cap H^1(\Omega)^3$ and $\mathcal{X}^0_\mathcal{E}$ coincide.

When Ω is non-convex, we shall suppose that Ω has N_{re} reentrant edges of dihedral angles $(\Theta_e=\pi/\alpha_e)_{e=1,\dots,\mathrm{N}_{re}}$, with $1/2<\alpha_e<1$. Let r_e denote the (orthogonal) distance to the reentrant edge e, and $r=\min\limits_{e=1,\dots,\mathrm{N}_{re}}r_e$.
Let $L^2_\gamma(\Omega)$ be the following weighted space, with $||\cdot||_{0,\gamma}$ norm:

$$L^2_\gamma(\Omega)=\{v\in L^2_{loc}(\Omega)\,|\,\int_\Omega(w_\gamma v)^2\,\mathrm{d}\Omega<\infty\}\,,\,||v||^2_{0,\gamma}=\int_\Omega(w_\gamma v)^2\,\mathrm{d}\Omega.$$

Above, the weight w_γ is a smooth non-negative function of $\mathbf{x}$. It behaves locally as r^γ in the neighborhood of the reentrant edges, and is bounded above and below by strictly positive constants outside the same neighborhood (this corresponds to the simplified weights of [19]). Under suitable data assumptions, $\mathcal{E}(t)\in\mathcal{X}^A_{\mathcal{E},\gamma}$, with:

$$\mathcal{X}^A_{\mathcal{E},\gamma}:=\{\mathcal{F}\in\mathcal{H}_A(\mathbf{curl},\Omega)\,|\,\mathrm{div}\mathcal{F}\in L^2_\gamma(\Omega)\}.$$

When $\Gamma_C=\partial\Omega$, we write $\mathcal{X}^0_{\mathcal{E},\gamma}$. According to Costabel and Dauge [19], there exists $\gamma_{min}\in]0,1/2[$ such that for all $\gamma\in]\gamma_{min},1[$:

- on $\mathcal{X}^0_{\mathcal{E},\gamma}$, the graph norm and the semi-norm:

$$||\mathcal{F}||^2_{\mathcal{X}^0_\gamma}=||\mathbf{curl}\mathcal{F}||^2_0+||\mathrm{div}\mathcal{F}||^2_{0,\gamma}$$

  are equivalent norms;
- $\mathcal{X}^0_{\mathcal{E},\gamma}\cap H^1(\Omega)^3$ is dense in $\mathcal{X}^0_{\mathcal{E},\gamma}$.

From a practical point of view, we remark that if one chooses any γ larger than $1/2$, then the results are valid *independently* of the geometry of the domain. In

particular, this allows us to work without the explicit knowledge of the form of the singular part of the field.

In the following, we shall write $L^2_{(\gamma)}(\Omega)$, $\mathcal{X}^0_{\mathcal{E}(,\gamma)}$ and $||\cdot||_{\mathcal{X}^0_{(\gamma)}}$ to handle both cases simultaneously, depending on whether the domain is convex or non-convex.

3. Variational formulations

Starting from the second-order in time system of equations (1.9-1.14), we obtain a series of equivalent variational formulations. When Γ_A is empty, we refer the interested reader to [25] for details. When Γ_A is non-empty, it is enough to adapt the proofs given by Ben Belgacem and Bernardi [8] to handle the boundary terms.

The basic Variational Formulation. Multiply eq. (1.9) by $\mathcal{F} \in \mathcal{H}_A(\mathbf{curl}, \Omega)$, and integrate by parts over Ω. We get the variational formulation (VF):
Find $\mathcal{E}(t) \in \mathcal{H}_A(\mathbf{curl}, \Omega)$ such that
$\forall \mathcal{F} \in \mathcal{H}_A(\mathbf{curl}, \Omega)$, $\forall t$,

$$\langle \partial_{tt}\mathcal{E}, \mathcal{F} \rangle + c^2(\mathbf{curl}\mathcal{E}, \mathbf{curl}\mathcal{F})_0 + c \int_{\Gamma_A} (\partial_t\mathcal{E} \times \mathbf{n}).(\mathcal{F} \times \mathbf{n}) \, d\Gamma$$

$$= -(\partial_t\mathcal{J}/\varepsilon_0, \mathcal{F})_0 - c \int_{\Gamma_A} (c\partial_t\mathbf{b} \times \mathbf{n}).\mathcal{F} \, d\Gamma. \qquad (3.1)$$

Above, $\langle \cdot, \cdot \rangle$ denotes an *ad hoc* duality product between $\partial_{tt}\mathcal{E}$ and elements of $\mathcal{H}_A(\mathbf{curl}, \Omega)$, cf. [8].

Theorem 3.1. *Suppose that $\partial_t\mathcal{J} \in L^2(0, T; L^2(\Omega)^3)$, $\rho \in \mathcal{C}^0(0, T; H^{-1}(\Omega))$, ρ and $\mathcal{J}$ satisfying (1.5). Suppose that $(\mathcal{E}_0, \mathcal{E}_1) \in \mathcal{H}_A(\mathbf{curl}, \Omega) \times L^2(\Omega)^3$.*
Then, equation (3.1), together with initial conditions (1.13-1.14), is equivalent to problem (PE) and has a unique solution $\mathcal{E}$ such that $(\mathcal{E}, \partial_t\mathcal{E}) \in C^0(0, T; \mathcal{H}_A(\mathbf{curl}, \Omega)) \times C^0(0, T; L^2(\Omega)^3)$.
Moreover, provided that $\rho \in \mathcal{C}^0(0, T; L^2_{(\gamma)}(\Omega))$ and $\mathcal{E}_0 \in \mathcal{X}^A_{\mathcal{E}(,\gamma)}$, we have the improved regularity result $\mathcal{E} \in C^0(0, T; \mathcal{X}^A_{\mathcal{E}(,\gamma)})$.

The Augmented Variational Formulation. Add $c^2(\mathrm{div}\mathcal{E}, \mathrm{div}\mathcal{F})_{0,(\gamma)}$ to the left-hand side of (3.1) and $c^2(\rho/\varepsilon_0, \mathrm{div}\mathcal{F})_{0,(\gamma)}$ to its right-hand side to get the following augmented VF (AVF):
Find $\mathcal{E}(t) \in \mathcal{X}^A_{\mathcal{E}(,\gamma)}$ such that
$\forall \mathcal{F} \in \mathcal{X}^A_{\mathcal{E}(,\gamma)}$, $\forall t$,

$$\langle \partial_{tt}\mathcal{E}, \mathcal{F} \rangle + c^2(\mathcal{E}, \mathcal{F})_{\mathcal{X}^0_{(\gamma)}} + c \int_{\Gamma_A} (\partial_t\mathcal{E} \times \mathbf{n}).(\mathcal{F} \times \mathbf{n}) \, d\Gamma$$

$$= -(\partial_t\mathcal{J}/\varepsilon_0, \mathcal{F})_0 + c^2(\rho/\varepsilon_0, \mathrm{div}\mathcal{F})_{0,(\gamma)} - c \int_{\Gamma_A} (c\partial_t\mathbf{b} \times \mathbf{n}).\mathcal{F} \, d\Gamma. \qquad (3.2)$$

Theorem 3.2. *Suppose that $\partial_t\mathcal{J} \in L^2(0, T; L^2(\Omega)^3)$, $\rho \in \mathcal{C}^0(0, T; L^2_{(\gamma)}(\Omega))$, ρ and $\mathcal{J}$ satisfying (1.5). Suppose that $(\mathcal{E}_0, \mathcal{E}_1) \in \mathcal{X}^A_{\mathcal{E}(,\gamma)} \times L^2(\Omega)^3$.*

6   *P. Ciarlet, Jr and E. Jamelot*

Then, equation (3.2), together with initial conditions (1.13-1.14), is equivalent to problem (PE) and has a unique solution $\mathcal{E}$ such that $(\mathcal{E}, \partial_t \mathcal{E}) \in C^0(0, T; \mathcal{X}^A_{\mathcal{E}(,\gamma)}) \times C^0(0, T; L^2(\Omega)^3)$.

The Mixed, Augmented Variational Formulation. Add a constraint on the divergence of $\mathcal{E}$ (cf. (1.10)), set in $L^2_{(\gamma)}(\Omega)$. If $p \in L^2_{(\gamma)}(\Omega)$ is the Lagrange multiplier, we reach the mixed AVF (MAVF) below, by adding[b] also $(p, \mathrm{div}\mathcal{F})_{0(,\gamma)}$ to the left-hand side of (3.2):
Find $(\mathcal{E}(t), p(t)) \in \mathcal{X}^A_{\mathcal{E}(,\gamma)} \times L^2_{(\gamma)}(\Omega)$ such that
$\forall \mathcal{F} \in \mathcal{X}^A_{\mathcal{E}(,\gamma)}, \forall t,$

$$\langle \partial_{tt}\mathcal{E}, \mathcal{F} \rangle + c^2(\mathcal{E}, \mathcal{F})_{\mathcal{X}^0_{(\gamma)}} + (p, \mathrm{div}\mathcal{F})_{0(,\gamma)} + c \int_{\Gamma_A} (\partial_t \mathcal{E} \times \mathbf{n}).(\mathcal{F} \times \mathbf{n}) \, \mathrm{d}\Gamma$$

$$= -(\partial_t \mathcal{J}/\varepsilon_0, \mathcal{F})_0 + c^2(\rho/\varepsilon_0, \mathrm{div}\mathcal{F})_{0(,\gamma)} - c \int_{\Gamma_A} (c\partial_t \mathbf{b} \times \mathbf{n}).\mathcal{F} \, \mathrm{d}\Gamma, \quad (3.3)$$

and $\forall q \in L^2_{(\gamma)}(\Omega), \forall t,$

$$(\mathrm{div}\mathcal{E}, q)_{0(,\gamma)} = (\rho/\varepsilon_0, q)_{0(,\gamma)}. \quad (3.4)$$

Theorem 3.3. *Suppose that $\partial_t \mathcal{J} \in L^2(0, T; L^2(\Omega)^3)$, $\rho \in C^0(0, T; L^2_{(\gamma)}(\Omega))$, ρ and $\mathcal{J}$ satisfying (1.5). Suppose that $(\mathcal{E}_0, \mathcal{E}_1) \in \mathcal{X}^A_{\mathcal{E}(,\gamma)} \times L^2(\Omega)^3$.*
Then, equations (3.3-3.4), together with initial conditions (1.13-1.14), are equivalent to problem (PE) and have a unique solution $(\mathcal{E}, p)$ such that $(\mathcal{E}, \partial_t \mathcal{E}) \in C^0(0, T; \mathcal{X}^A_{\mathcal{E}(,\gamma)}) \times C^0(0, T; L^2(\Omega)^3)$ and $p = 0$.

The constraint (3.4) is added to reinforce Gauss' law and also to avoid numerical instabilities when the discrete charge conservation equation is not satisfied while solving the Maxwell-Vlasov system. Actually, if the charge conservation does not hold, the Lagrange multiplier no longer vanishes, and it compensates for the discrepancy [7].

One can build a similar VF, AVF, or MAVF, for the magnetic field. Some examples are provided in Section 5, with the AVFs (5.2) and (5.3).

4. Discretization

To build discretized (M)AVFs, let us begin with a semi-discretization in time. Since the difficulty lies in the approximation of the fields in space, we choose simple (yet at the same time reliable) schemes in time, the explicit centered schemes of order two. If we let Δt be the time-step and $t_n = n\Delta t$, $n \in \mathbb{N}$, be the discrete times, we consider respectively that

- $\partial_t u(., t_n)$ is approximated by $[u(., t_{n+1}) - u(., t_{n-1})]/(2\Delta t)$;

[b]Evidently, one expects that $p = 0$, since the mapping div : $\mathcal{X}^A_{\mathcal{E}(,\gamma)} \to L^2_{(\gamma)}(\Omega)$ is onto!

- $\partial_{tt}u(.,t_n)$ is approximated by $[u(.,t_{n+1}) - 2u(.,t_n) + u(.,t_{n-1})]/\Delta t^2$.

In space, we consider meshes made of tetrahedra and use the conforming, continuous[c] P_k Lagrange Finite Element to discretize the AVF, and the P_{k+1}-P_k conforming, continuous[c] Taylor-Hood Finite Element to discretize the MAVF. We denote by h the meshsize. So, one has to compute the approximations $\mathcal{E}_h^n$ and p_h^n, for n such that $0 \leq n \leq T/\Delta t$.

Recall that for the fully discretized explicit scheme, one must satisfy a CFL-like condition. For the P_k FE, we must have $c\Delta t \leq C_k \min_l \rho_l$, where the value C_k depends on the order of the FE, and, if T_l is the lth tetrahedron, $\rho_l = \sup\{\text{diam}(S) : S \text{ is a ball contained in } T_l\}$.

Since we introduce conforming, continuous approximations of the field in space, we refer to these discretization methods as *continuous Galerkin methods*.

4.1. *Error estimates*

For the sake of completeness, we report here some error estimate results for the discretization of the Augmented Variational Formulation. When one solves the time-harmonic [19], or the static [25], Maxwell equations, one gets

$$||\mathcal{E} - \mathcal{E}_h||_{\mathcal{X}_\gamma^0} \leq C_\varepsilon h^{\gamma - \gamma_{min} - \varepsilon}, \ \forall \varepsilon > 0.$$

Accompanying this estimate, one should note first that this estimate is *independent* of the singular part of the electric field $\mathcal{E}$. As a matter of fact, it depends only on the geometry via the exponent γ_{min}. Then, if γ increases, the convergence rate *improves*, the trade-off being that the norm in which the error is measured is *weaker*. Finally, this is a *worst case* estimate, in the sense that if the electric field is smooth, one recovers an improved convergence rate (using standard estimates, up to Ch^l with $l = k$ or $k + 1$, since we discretized in space with the P_k or P_{k+1} continuous Finite Elements).

Concerning error estimate results for the time-dependent Maxwell equations with the centered explicit scheme, one can reach the standard[26] estimate

$$\max_n \left(||\mathcal{E}(t_n) - \mathcal{E}_h^n||_0\right) \leq C_\varepsilon \left((\Delta t)^2 + h^{\gamma - \gamma_{min} - \varepsilon}\right), \ \forall \varepsilon > 0.$$

Additionally, we note that if one considers an *implicit scheme* such as the Crank-Nicholson scheme, one can obtain, following [16], the result

$$\max_n \left(||\partial_t \mathcal{E}(t_n) - \partial_\tau \mathcal{E}_h^n||_0^2 + c^2||\mathcal{E}(t_n) - \mathcal{E}_h^n||_{\mathcal{X}_\gamma^0}^2\right)$$
$$\leq C_\varepsilon \left((\Delta t)^2 + h^{2(\gamma - \gamma_{min} - \varepsilon)} + (\Delta t)^2 h^{2(\gamma - \gamma_{min} - 1 - \varepsilon)}\right), \ \forall \varepsilon > 0,$$

---

[c]By construction, the discretized field and the test-fields are continuous, and piecewise smooth. So, they belong naturally to $H^1(\Omega)^3$. Since the discretization method is conforming, they also belong to $\mathcal{X}_{\mathcal{E}(,\gamma)}^A$. Then, in order to be able to apply the classical Galerkin theory, a necessary condition is that $\mathcal{X}_{\mathcal{E}(,\gamma)}^A \cap H^1(\Omega)^3$ be *dense* in $\mathcal{X}_{\mathcal{E}(,\gamma)}^A$.

where $\partial_\tau \mathcal{E}_h^n = [\mathcal{E}_h^n - \mathcal{E}_h^{n-1}]/\Delta t$.

4.2. *Numerical resolution*

We now proceed with the construction of the actual series of linear systems that one has to solve to compute the discrete solution over the discrete times, i. e. as long as $t_n \leq T$. Let N_k (resp. N_{k+1}) be the number of P_k (resp. P_{k+1}) degrees of freedom. Then, the discretized electric field (resp. the discretized Lagrange multiplier) at time t_n can be represented by $\vec{E}^n \in (\mathbb{R}^3)^{N_{k+1}}$ (resp. $\vec{p}^n \in \mathbb{R}^{N_k}$). Let $\mathbb{M}_\Omega \in (\mathbb{R}^{3\times3})^{N_{k+1}\times N_{k+1}}$ be the mass matrix, and $\mathbb{M}_{\Gamma_A}^{\parallel} \in (\mathbb{R}^{3\times3})^{N_{k+1}\times N_{k+1}}$ be the boundary mass matrix, defined on Γ_A. Let $\mathbb{C} \in (\mathbb{R}^{1\times3})^{N_k \times N_{k+1}}$ be the constraint matrix. At time t_n, we have to solve:

$$\left(\mathbb{M}_\Omega + \frac{c\Delta t}{2}\mathbb{M}_{\Gamma_A}^{\parallel}\right)\vec{E}^{n+1} + (\Delta t)^2 \mathbb{C}^T \vec{p}^{n+1} = \vec{F}^{n+1/2}\,,$$
$$\mathbb{C}\vec{E}^{n+1} = \vec{G}^{n+1}\,. \qquad (4.1)$$

Let $\mathbb{M} = \mathbb{M}_\Omega + \frac{1}{2}c\Delta t\mathbb{M}_{\Gamma_A}^{\parallel}$. The algorithm is the following:

- solve first $\mathbb{M}\vec{E}_0^{n+1} = \vec{F}^{n+1/2}$,
- then $\mathbb{C}\mathbb{M}^{-1}\mathbb{C}^T\vec{p}^{n+1} = \mathbb{C}\vec{E}_0^{n+1} - \vec{G}^{n+1}$,
- and finally $\mathbb{M}\vec{E}^{n+1} = \mathbb{M}\vec{E}_0^{n+1} - \mathbb{C}^T\vec{p}^{n+1}$.

The Lagrange multiplier $\vec{p}^{n+1}$ may be computed with an iterative algorithm, similar to the Uzawa algorithm. To be more precise, one can use the Preconditioned Conjugate Gradient Method, taking the P_k mass matrix as the preconditioner, or even a "diagonalized" P_k mass matrix (by a lumping technique, see below). When the domain is convex, it is proven in [25] that this yields an optimal method, in terms of the number of iterations: in other words, this number does not depend on the meshsize h. When the domain is not convex, it has been observed numerically that this number of iterations grows, albeit very slowly, when h decreases. Moreover, in practice, given a mesh made of tetrahedra with good aspect ratio, it has been noted [21] that $\vec{p}^{n+1}$ does not vary much (from the zero theoretical value), so that there is actually no need to compute it at all times. However, if there is a coupling with the Vlasov equation, one has to compute accurately[7] this Lagrange multiplier.

To speed up the resolution further, one can perform the so-called mass-lumping techniques, to obtain diagonal mass matrices in (4.1). It has been established in [17] that this could be achieved, for a *continuous discretization*, with no loss in accuracy. This results in the so-called $\widetilde{P}_1$ or $\widetilde{P}_2$ Finite Elements. In the latter case, accuracy is preserved at the cost of increasing the total number of degrees of freedom, going from 10 dof for the P_2 FE to 23 dof for the $\widetilde{P}_2$ FE. In the former case, the number of dof is equal to four for both the P_1 and the $\widetilde{P}_1$ FEs.

5. Numerical results

We present two test-cases below. The first one is classical [23], and deals with the accurate resolution of cavity modes, in a bounded, convex domain. The second one is aimed at proving that one can capture the singular behavior (with respect to **x**) of the time-dependent electric field, with the help of the continuous Galerkin method we introduced before. We study the propagation of the field, generated by an oscillating current, in a non-convex domain (the geometrical singularity is made of an edge).

We encoded the problem in Fortran 77.

5.1. *Example: a convex geometry*

The domain $\Omega^{(1)}$ is the unit cube, with dimension $L = 1$ m, and it is enclosed by a perfect conductor, so that its boundary $\partial\Omega^{(1)}$ reduces to $\Gamma_C^{(1)}$. The data is made of zero charge and current densities $(\rho, \mathcal{J}) = (0, 0)$, and non-zero initial conditions $(\mathcal{E}_0, \mathcal{B}_0)$:

$$\mathcal{E}_0 = \begin{pmatrix} \cos(\pi x)\,\sin(\pi y)\,\sin(-2\pi z) \\ \sin(\pi x)\,\cos(\pi y)\,\sin(-2\pi z) \\ \sin(\pi x)\,\sin(\pi y)\,\cos(-2\pi z) \end{pmatrix} , \mathcal{B}_0 = 0.$$

Note that $\mathcal{E}_0$ and $\mathcal{B}_0$ are divergence-free by construction, and that they satisfy the boundary conditions (1.7). The AVF in $\mathcal{E}$ reduces to the following
Find $\mathcal{E}(t) \in \mathcal{X}_{\mathcal{E}}^0$ *such that*

$$\forall \mathcal{F} \in \mathcal{X}_{\mathcal{E}}^0, \ \forall t, \quad \langle \partial_{tt}\mathcal{E}, \mathcal{F} \rangle + c^2 (\mathcal{E}, \mathcal{F})_{\mathcal{X}^0} = 0. \tag{5.1}$$

Similarly, one can write an AVF for the magnetic induction $\mathcal{B}$, set in

$$\mathcal{X}_{\mathcal{B}}^0 := \{\mathcal{C} \in \mathcal{H}(\mathbf{curl}, \Omega) \,|\, \mathrm{div}\mathcal{C} \in L^2(\Omega)\,, \mathcal{C} \cdot \mathbf{n}_{|\partial\Omega} = 0\}.$$

In this functional space, $|| \cdot ||_{\mathcal{X}^0}$ is still a relevant choice (see [18]). The AVF in $\mathcal{B}$ is:
Find $\mathcal{B}(t) \in \mathcal{X}_{\mathcal{B}}^0$ *such that*

$$\forall \mathcal{C} \in \mathcal{X}_{\mathcal{B}}^0, \ \forall t, \quad \langle \partial_{tt}\mathcal{B}, \mathcal{C} \rangle + c^2 (\mathcal{B}, \mathcal{C})_{\mathcal{X}^0} = 0. \tag{5.2}$$

It can be checked that the exact solution is (with $\omega = \sqrt{6}\pi\, cL^{-1} \approx 2.3$ GHz),

$$\mathcal{E}(t) = \cos(\omega t) \begin{pmatrix} \cos(\pi x)\,\sin(\pi y)\,\sin(-2\pi z) \\ \sin(\pi x)\,\cos(\pi y)\,\sin(-2\pi z) \\ \sin(\pi x)\,\sin(\pi y)\,\cos(-2\pi z) \end{pmatrix} ,$$

$$\mathcal{B}(t) = \frac{3\,\pi}{\omega} \sin(\omega t) \begin{pmatrix} -\sin(\pi x)\,\cos(\pi y)\,\cos(-2\pi z) \\ \cos(\pi x)\,\sin(\pi y)\,\cos(-2\pi z) \\ 0 \end{pmatrix} .$$

The computations have been carried out on a tetrahedral mesh, with 24 576 tetrahedra ($\min_l \rho_l \approx 2.8$ cm). With roughly 30 discretization points per unit length, the ten discretization points per wavelength rule of thumb is fulfilled ($\lambda_x = \lambda_y = 2$ m,

$\lambda_z = 1$ m). To observe a complete oscillation, we chose $T = 4$ ns. We implemented the P_1, $\widetilde{P}_1$ and P_2 Lagrange Finite Elements. To comply with the CFL stability condition, we considered a time-step $\Delta t \approx 47$ ps for the P_1 and $\widetilde{P}_1$ FEs, and $\Delta t \approx 4.7$ ps for the P_2 FE.

First, we plot results, in which we compare the different discretizations obtained for the three choices of FE over the discrete times, to the exact solution. Due to the symmetry of the problem, the three components of the field behave similarly. We focus on the component $\mathcal{E}_y$, at the location $(0.19, 0.12, 0.12)$. Up to the numerical
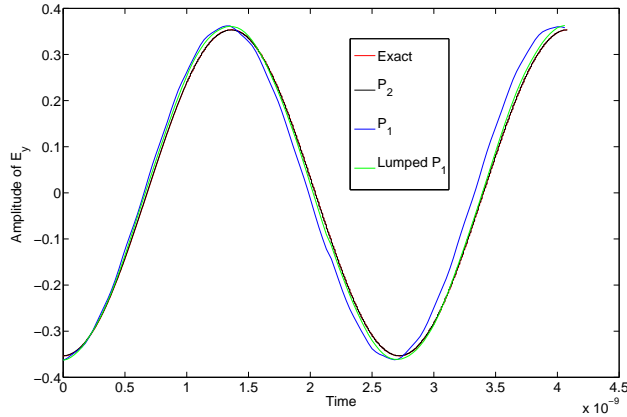
Fig. 1. Relative amplitudes of $\mathcal{E}_y$ at location $(0.19, 0.12, 0.12)$.

accuracy in Figure 1 (about 0.1%), the P_2 numerical approximation coincides with the exact solution. As far as the P_1 and $\widetilde{P}_1$ approximations are concerned, we observe a slight variation in the amplitude, albeit smaller for the $\widetilde{P}_1$ discrete field. Also, a phase shift appears for both methods, as is expected, cf. [17]. Results are very similar for the magnetic induction.

Second, we examine the evolution of the discrete energy. Let W_B^n be the discrete energy at the discrete time t_n, which one recalls is measured in the $\mathcal{X}_\mathcal{B}^0$-norm, so that it is equal to,

$$W_B^n = \frac{1}{2} \left(\|\partial_\tau \mathcal{B}_h^{n+1}\|_0 + c^2 (\mathcal{B}_h^{n+1}, \mathcal{B}_h^n)_{\mathcal{X}^0} \right).$$

For the P_1 discretization of the magnetic induction, one finds that

$$\max_n \frac{|W_B^n - W_B^0|}{W_B^0} \leq 3.10^{-12},$$

which validates the expected conservation of the discrete energy.

Finally, we study the evolution in time of the discrete divergence, which belongs to $L^2(\Omega^{(1)})$ by construction (since the method is conforming in $\mathcal{X}_{\mathcal{B}}^0$). In Figure 2, we plot the L^2-norm of the difference of the exact and discrete divergences of the magnetic induction (recall that $\text{div}\mathcal{B} = 0$) over the discrete times, normalized by the discrete energy W_B^0. The error oscillates, but remains lower than 1%. Heuristically,
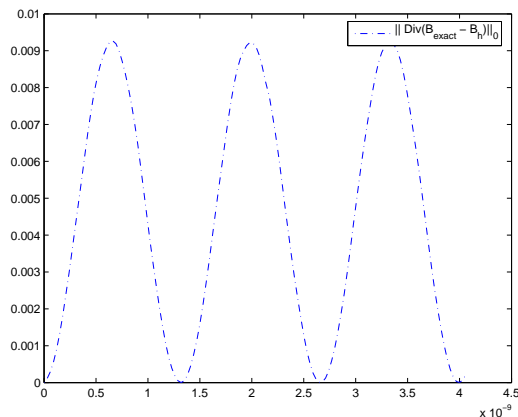

Fig. 2. Evolution in time of the error in the divergence.

this is due to the fact that we have used a mesh made of tetrahedra with good aspect ratios. In this case, the use of the Lagrange multiplier at the discrete level is not necessary.

5.2. *Example: a non-convex geometry*

The domain $\Omega^{(2)}$ is an extruded, L-shaped, polyhedron (see Figure 3), of depth $L = 4$ m. Geometrically speaking, its boundary $\partial\Omega^{(2)}$ has a single reentrant edge of dihedral angle $2\pi/3$, so that $\alpha = 2/3$. In this case, it can be checked that $\gamma_{min} = 1 - \alpha = 1/3$. Physically speaking, the boundary is split in two parts, $\Gamma_C^{(2)}$ and $\Gamma_A^{(2)}$. The latter is composed of the leftmost and rightmost faces of the boundary. Further, the Silver-Müller boundary condition (1.8) on the artificial boundary $\Gamma_A^{(2)}$ holds with $\mathbf{b} = 0$: we impose an absorbing condition. The data is made of zero initial conditions $(\mathcal{E}_0, \mathcal{B}_0)$, and non-zero charge and current densities $(\rho, \mathcal{J})$. A current bar B_J crosses the domain, and inside this bar, there holds (with $\omega = 2.5$ GHz)

$$\mathcal{J} = 10^{-5}\omega \sin(\pi z/L)\cos(\omega t)\mathbf{z}\,,\ \rho = 10^{-5}(\pi/L)\cos(\pi z/L)\sin(\omega t).$$

The wavelength and time period associated to ω are respectively equal to $2\pi c/\omega \approx 0.75$ m and $2\pi/\omega \approx 2.5$ ns. It is clear that the dimensions of our domain are not realistic, however we made this choice in order to be able to visualize several
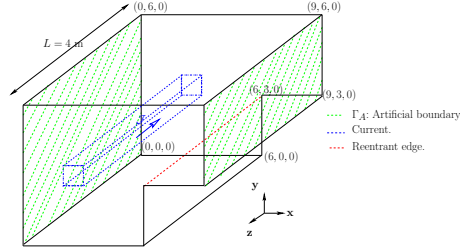
12   *P. Ciarlet, Jr and E. Jamelot*

Fig. 3. The model problem.

oscillations of the field (in space).

We note that both $\mathcal{J}$ and ρ are smooth, so all Theorems of Section 3 apply, which ensures theoretically the existence and uniqueness of the electromagnetic field. To compute the electric field, we considered the space $\mathcal{X}^A_{\mathcal{E},\gamma}$, with $\gamma = 0.95$, and the AVF (3.2). The value of the exponent $\gamma - \gamma_{min}$ that appears in the convergence rates is then approximately equal to 0.62. To compute the magnetic induction, we introduced (again with $\gamma = 0.95$)

$$\mathcal{X}^A_{\mathcal{B},\gamma} := \{\mathcal{C} \in \mathcal{H}(\mathbf{curl}, \Omega) \,|\, \mathrm{div}\mathcal{C} \in L^2_\gamma(\Omega)\,,\, \mathcal{C} \times \mathbf{n}_{|\partial\Omega} \in \mathcal{L}^2_t(\partial\Omega)\,,\, \mathcal{C} \cdot \mathbf{n}_{|\Gamma_C} = 0\}.$$

The corresponding AVF in $\mathcal{B}$ is then as follows

Find $\mathcal{B}(t) \in \mathcal{X}^A_{\mathcal{B},\gamma}$ such that

$\forall \mathcal{C} \in \mathcal{X}^A_{\mathcal{B},\gamma}$, $\forall t$,

$$\langle \partial_{tt}\mathcal{B}, \mathcal{C} \rangle + c^2(\mathcal{B}, \mathcal{C})_{\mathcal{X}^0_\gamma} + c \int_{\Gamma_A} (\partial_t \mathcal{B} \times \mathbf{n}).(\mathcal{C} \times \mathbf{n}) \, d\Gamma = \frac{1}{\varepsilon_0}(\mathcal{J}, \mathbf{curl}\mathcal{C})_{\mathcal{X}^0_\gamma}. \qquad (5.3)$$

We report the results of computations made with the $\widetilde{P}_1$ FE on a tetrahedral mesh, with 685 000 tetrahedra. In particular, the ten discretization point per wavelength rule is satisfied. One has $\min_l \rho_l \approx 6$ cm, and the time-step is in the order of $\Delta t \approx 40$ ps: this complies with the CFL condition. The final observation time is $T = 25$ ns: it is sufficient for the electromagnetic wave that is generated by B_J to span the whole domain (recall that the wave travels at the finite speed $c \approx 3.10^8\,\mathrm{m.s}^{-1}$).

On Figure 4, we present the time evolution of the x-component of the electric field at the locations $M_1 = (1, 1, 2)$, $M_2 = (5.5, 2.5, 2)$, $M_3 = (1, 1, 2)$ and $M_4 = (8, 5.5, 2)$ respectively. It remains equal to zero until the electric wave reaches the point under consideration. Then the field oscillates with a period ≈ 2.5 ns: as expected, we observe forced oscillations.

Let us now focus on the spatial behavior of the electromagnetic field, which we expect to be singular [d], in the neighborhood of the reentrant edge. We report the

---

[d] According to physics principles, to experiments, and also to the mathematical theory.
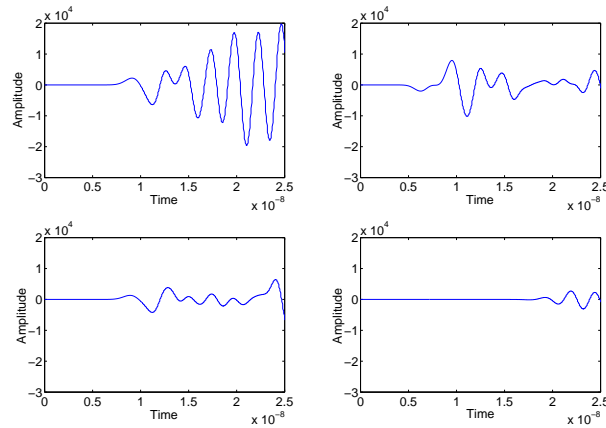
Fig. 4. $\mathcal{E}_x$ at locations $(M_i)_{1 \le i \le 4}$.

evolution of the field in a plane, which is perpendicular to that edge: the geometrical singularity projects to a reentrant corner.

On Figures 5 and 6, the space evolution of the x- and y-components of the electric field is represented in the plane $z = 2.5$ m, at times $T_1 = 1$ ns, $T_2 = 8$ ns, $T_3 = 15$ ns, $T_4 = 20$ ns. We can see that an electric wave is created by the current, that it propagates into the cavity with wavelength ≈ 0.75 m, and is reflected by the conductor as expected. At T_3, we observe a growing peak of intensity close to the reentrant corner.
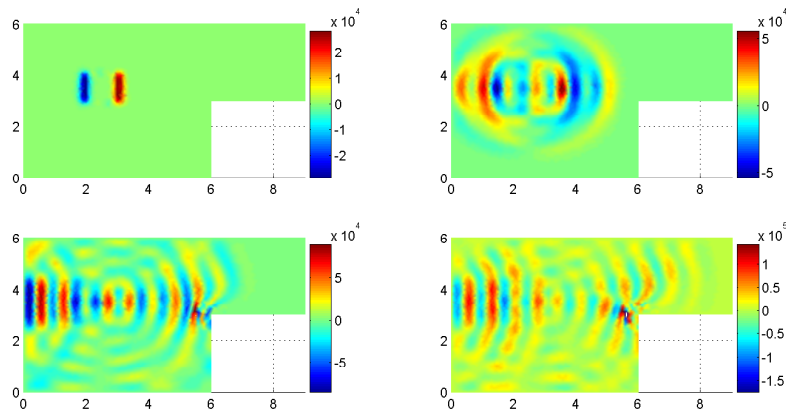
Fig. 5. $\mathcal{E}_x$ at times $(T_i)_{1 \le i \le 4}$, in the plane $z = 2, 5$ m.
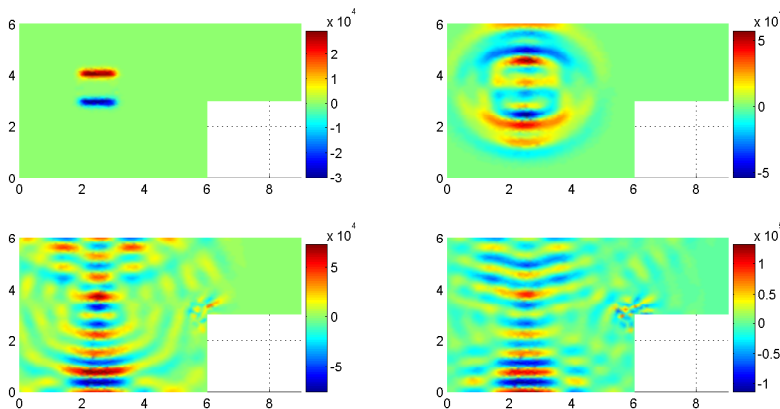
Fig. 6. $\mathcal{E}_y$ at times $(T_i)_{1\leq i\leq 4}$, in the plane $z = 2,5$ m.

We also provide a close up of the x-component near the reentrant corner on Figure 7, again at times T_i, $i = 1, 4$. The usual pattern of strong variations is visible, once the wave has reached the corner, especially at time T_3.
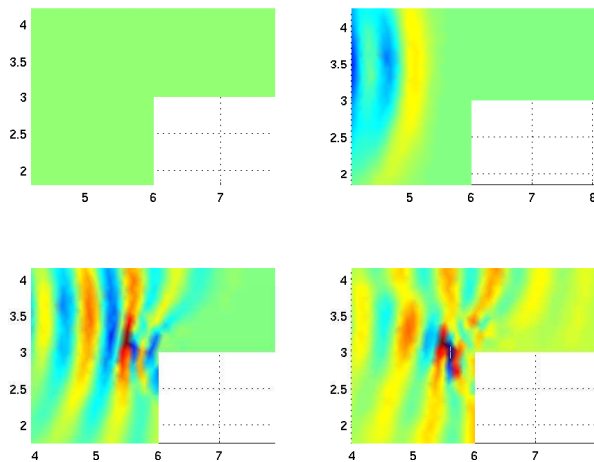

Fig. 7. A close-up of $\mathcal{E}_x$ at times $(T_i)_{1\leq i\leq 4}$, in the plane $z = 2,5$ m.

On Figure 8, we picture the space evolution of the z-component in the plane $z = 2.5$ m, at times T_i, $i = 1, 4$. Again, we observe the propagation of the wave with wavelength ≈ 0.75 m, and the reflections. Note that this component is always regular (as opposed to singular), which is due to the fact that the geometrical singularity is parallel the z-axis [12,14]. Moreover, it takes smaller (absolute) values
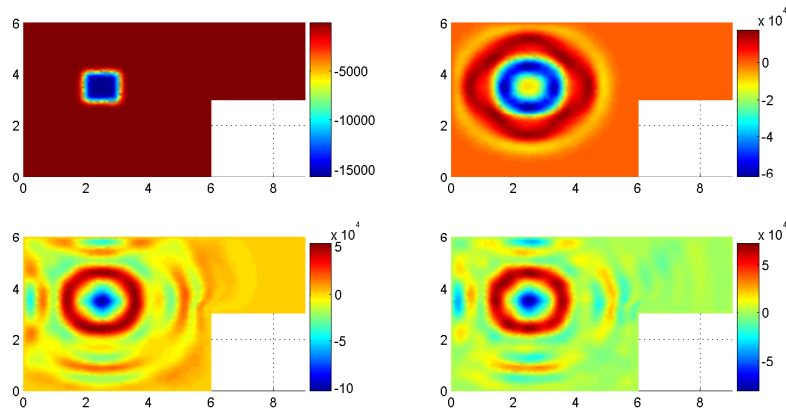
than the x and y-components.

Fig. 8. $\mathcal{E}_z$ at times $(T_i)_{1 \leq i \leq 4}$, in the plane $z = 2, 5$ m.

On Figures 5, 6 and 8, one can see spurious reflections on Γ_A, due to the fact that the Silver-Müller boundary condition is simply of first order: only plane waves with normal incidence are absorbed, which is not our case.

As far as the magnetic induction is concerned, we observe a similar behavior up to a rotation of $\pi/2$ around the z-axis. So for instance, we show on Figure 9 the space evolution of $\mathcal{B}_y$ in the plane $z = 2.5$ m, at times T_i, $i = 1, 4$.

Physically speaking, the overall space distribution of the electromagnetic field can be explained with the help of the Biot-Savart law. According to this law, the magnetic induction created by the current bar B_J at location M reads

$$\mathcal{B}(M) = \frac{\mu_0}{4\pi} \int_{B_J} \frac{\mathcal{J} \times \overrightarrow{PM}}{|\overrightarrow{PM}|^2} \, d\Omega_{(P)}.$$

Thus, at location M, one has $\mathcal{B}(M) \propto \dfrac{\mathcal{J} \times \overrightarrow{M'M}}{|\overrightarrow{M'M}|^2}$, where M' is the orthogonal projection of M on the $(z$-)axis of B_J. Let (x, y, z) be the coordinates of M, and let (x', y', z) be those of M'. One gets

$$\mathcal{B}(M) \propto \frac{\mathcal{J}_z}{|\overrightarrow{M'M}|^2} \begin{pmatrix} -(y-y') \\ (x-x') \\ 0 \end{pmatrix}.$$

Therefore, if $y = y'$, $\mathcal{B}_x(M) \approx 0$, whereas if $x = x'$, $\mathcal{B}_y(M) \approx 0$. On Figure 9, one sees in particular that, at time T_1, $\mathcal{B}_y$ vanishes vertically, i. e. for those locations
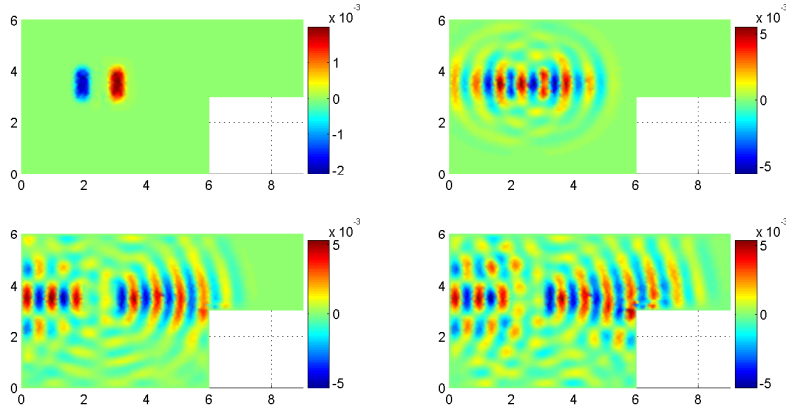
16   *P. Ciarlet, Jr and E. Jamelot*

Fig. 9. $\mathcal{B}_y$ at times $(T_i)_{1 \le i \le 4}$, in the plane $z = 2, 5$ m.

M such that $x = x'$, that is above and below the current bar B_J. The electric field being orthogonal to the magnetic induction, one gets that if $y = y'$, $\mathcal{E}_y(M) \approx 0$, whereas if $x = x'$, $\mathcal{E}_x(M) \approx 0$. This can be observed on Figures 5 and 6.

Numerically speaking, we note that if one implements the AVFs with the plain scalar product $(\cdot, \cdot)_{\mathcal{X}^0}$ instead of the weighted $(\cdot, \cdot)_{\mathcal{X}^0_\gamma}$, one gets similar numerical results until the wave hits the reentrant edge. This is a consequence of the fact that before that time, the fields are H^1-regular: both AVFs have the same solution. After that, the fields become singular, and results differ considerably: first, in the neighborhood of this edge, and this discrepancy extends in space at the speed of light c. This is due to the fact that the AVF with the plain scalar product $(\cdot, \cdot)_{\mathcal{X}^0}$ *can not* capture the singular part of the fields. In other words, it is crucial that one uses the correct variational formulation, in the correct functional space.

6. Conclusion

We presented results concerning a conforming, continuous approximation of the time-dependent electromagnetic field in 3D, polyhedral geometries. To the authors' knowledge, this is the first time 3D, time-dependent, singular electromagnetic fields are computed accurately with this type of approximation. We dealt successively with theoretical aspects and numerical algorithms, which we validated with the help of some numerical experiments. When the domain is convex, it corresponds to the method introduced by Heintzé *et al* [23,5]. When the domain is non-convex (and has a piecewise smooth boundary), the mathematical and numerical tools have been obtained within the framework developed by Costabel and Dauge [19] for the time-harmonic equations. In particular, knowledge of the singular part of the fields is not required. Should a constraint on the divergence be taken into account explicitly, the

Mixed, Augmented Variational Formulation we introduced can be used.

We note that when the computational domain is not simply connected, or when its boundary is not connected, one can use the theory developed in [1] to build well-posed variational formulations. Their discretization is then identical to what was proposed in this paper. In order to avoid spurious reflections, we suggest to use perfectly matched layers [9,10]. Finally, for the resolution of the $2D$ Maxwell equations with continuous Galerkin finite elements, we refer the reader to [21,25].

References

1. Amrouche, C., Bernardi, C., Dauge, M., Girault, V.: Vector potentials in three-dimensional non-smooth domains. Math. Meth. Appl. Sci., **21**, 823–864 (1998)
2. Assous, F., Ciarlet, Jr, P., Garcia, E., Segré, J.: Time-dependent Maxwell's equations with charges in singular geometries. Comput. Methods Appl. Mech. Engrg., **196**, 665–681 (2006)
3. Assous, F., Ciarlet, Jr, P., Labrunie, S., Segré, J.: Numerical solution to the time-dependent Maxwell equations in axisymmetric singular domains: the singular complement method. J. Comput. Phys., **191**, 147–176 (2003)
4. Assous, F., Ciarlet, Jr, P., Segré, J.: Numerical solution to the time-dependent Maxwell equations in two-dimensional singular domains: the singular complement method. J. Comput. Phys., **161**, 218–249 (2000)
5. Assous, F., Degond, P., Heintzé, E., Raviart, P.-A., Segré, J.: On a finite element method for solving the three-dimensional Maxwell equations. J. Comput. Phys., **109**, 222–237 (1993)
6. Assous, F., Degond, P., Segré, J.: Numerical approximation of the Maxwell equations in inhomogeneous media by a P_1 conforming finite element method. J. Comput. Phys., **128**, 363–380 (1996)
7. Barthelmé, R., Ciarlet, Jr, P., Sonnendrücker, E.: Generalized formulations of Maxwell's equations for numerical Vlasov-Maxwell simulations. *Math. Models Meth. App. Sci.*, **17(5)**, (2007)
8. Ben Belgacem, F., Bernardi, C.: Spectral element discretization of the Maxwell equations. Math. Comp., **68**, 1497–1520 (1999)
9. Bérenger, J.-P.: A perfectly matched layer for the absorption of electromagnetic waves. J. Comput. Phys., **114**, 185–200 (1994)
10. Bérenger, J.-P.: Three-dimensional perfectly matched layer for the absorption of electromagnetic waves. J. Comput. Phys., **127**, 363–379 (1996)
11. Birdsall, C. K., Langdon, A. B.: Plasma physics via computer simulation, Chapter 15. McGraw-Hill, New-York (1985)
12. Buffa, A., Costabel M., Dauge M.: Anisotropic regularity results for Laplace and Maxwell operators in a polyhedron. C. R. Acad. Sci. Paris, Ser I, **336**, 565–570 (2003)
13. Ciarlet, Jr, P.: Augmented formulations for solving Maxwell equations. Comp. Meth. Appl. Mech. and Eng., **194**, 559–586 (2005)
14. Ciarlet, Jr, P., Garcia, E., Zou, J.: Solving Maxwell equations in $3D$ prismatic domains. C. R. Acad. Sci. Paris, Ser. I, **339**, 721–726 (2004)
15. Ciarlet, Jr, P., Jamelot, E.: Continuous Galerkin methods for solving Maxwell equations in 3D geometries. Proccedings of ENUMATH 2005, Eds. A. Bermudez de Castro *et al*, Santiago de Compostela, Spain, Springer, p. 547-554 (2006)
16. Ciarlet, Jr, P., Zou, J.: Fully discrete finite element approaches for time-dependent Maxwell's equations. Numer. Math., **82**, 193–219 (1999)

18   *P. Ciarlet, Jr and E. Jamelot*

17. Cohen, G.: Higher-Order Numerical Methods for Transient Wave Equations, Chapters 11 & 12. Scientific Computation Series. Springer-Verlag, Berlin (2002)
18. Costabel, M.: A coercive bilinear form for Maxwell's equations. J. Math. An. Appl., **157**, 527–541 (1991)
19. Costabel, M., Dauge, M.: Weighted regularization of Maxwell equations in polyhedral domains. Numer. Math., **93**, 239–277 (2002)
20. Fernandes, P., Gilardi, G.: Magnetostatic and electrostatic problems in inhomogeneous anisotropic media with irregular boundary and mixed boundary conditions. Math. Models Meth. App. Sci., **7**, 957–991 (1997)
21. Garcia, E.: Solution to the instationary Maxwell equations with charges in non-convex domains (in French). PhD thesis, Université Paris VI, France (2002)
22. Hazard, C., Lohrengel, S.: A singular field method for Maxwell's equations: numerical aspects for 2D magnetostatics. SIAM J. Appl. Math., **40**, 1021-1040 (2002)
23. Heintzé, E.: Solution to the 3D instationary Maxwell equations with conforming finite elements (in French). PhD thesis, Université Paris VI, France (1992)
24. Jamelot, E.: Éléments finis nodaux pour les équations de Maxwell. C. R. Acad. Sci. Paris, Sér. I, **339**, 809–814 (2004)
25. Jamelot, E.: Solution to Maxwell equations with continuous Galerkin finite elements (in French). PhD thesis, École Polytechnique, Palaiseau, France (2005)
26. Raviart, P.-A., Thomas, J.-M.: Introduction à l'analyse numérique des équations aux dérivées partielles, Chapter 8. Masson, Paris (1983)